Gauge conditions for binary black hole puncture data based on an approximate helical Killing vector

Wolfgang Tichy, Bernd Brügmann, Pablo Laguna
Center for Gravitational Physics and Geometry and Center for Gravitational Wave Physics
Penn State University, University Park, PA 16802
(Dated: June 3, 2003)

We show that puncture data for quasicircular binary black hole orbits allow a special gauge choice that realizes some of the necessary conditions for the existence of an approximate helical Killing vector field. Introducing free parameters for the lapse at the punctures we can satisfy the condition that the Komar and ADM mass agree at spatial infinity. Several other conditions for an approximate Killing vector are then automatically satisfied, and the 3-metric evolves on a timescale smaller than the orbital timescale. The time derivative of the extrinsic curvature however remains significant. Nevertheless, quasicircular puncture data are not as far from possessing a helical Killing vector as one might have expected.

PACS numbers: 04.20.Ex, 04.25.Dm, 04.30.Db, 04.70.Bw

I. INTRODUCTION

Binary black hole (BH) mergers are among the most promising sources for the ground-based interferometric gravitational wave detectors GEO600, LIGO and TAMA [1], which have started to collect data. Predicting the gravitational waves from the dynamic and non-linear regime of BH mergers requires numerical simulation, and a crucial issue is to find astrophysically realistic initial data. This is a non-trivial task which involves specification of some appropriate free data and the solution of the constraint equations of general relativity for the remaining data. By now several methods to produce initial data for binary BH systems exist (see [2] for a recent review). However, there are still open issues concerning the construction of astrophysically realistic initial data, which in particular are data that represent two BHs on almost circular orbits during their inspiral, and furthermore data that represent a quantifiable approximation to two BHs near the transition from inspiral to plunge and merger.

During the inspiral, we expect the two BHs to be in quasicircular orbits around each other with a radius which shrinks on a timescale much larger than the orbital timescale. This means that the initial data should have an approximate helical Killing vector ξ. In addition one would like to have the initial data in coordinates such that this approximate symmetry is manifest, i.e. the time evolution vector should lie along ξ, so that the time derivatives of the evolved quantities are minimized. Then we would get

$$\partial_t g_{ij} \approx \partial_t \phi \approx \partial_t K \approx \partial_t A_{ij} \approx 0, \tag{1}$$

where we have decomposed the metric into a conformal factor ϕ and a conformal metric g_{ij}, and split the extrinsic curvature into its trace K and a tracefree piece A_{ij}. All the terms in Eq. (1) are of the order of some error quantity which measures the failure of an exact helical Killing vector to exist. This error has a finite value near the "innermost stable circular orbit" and tends to zero for increasing separation of the BHs. In principle one can improve the approximation by replacing the circular orbits by inspiraling orbits defined by a small but nonzero value of all the time derivatives in Eq. (1) based on post-Newtonian approximations, see for example [3].

One approach to construct quasicircular initial data is to use the conformal thin sandwich (CTS) decomposition [4, 5]. For CTS data the time derivative of the conformal metric is free data that can be set to zero. If in addition a maximal slicing lapse is used, one obtains $\partial_t g_{ij} = \partial_t K = 0$. Note, however, that $\partial_t \phi$ and $\partial_t A_{ij}$ are in general non-zero, since CTS by itself does not contain conditions concerning helical Killing vectors. In the case of the Meudon data [6, 7] (but see also [8, 9]), CTS data is constructed under the assumptions of a two-sheeted topology with isometry, a conformally flat 3-metric, and a vanishing K. In addition, in order to construct quasicircular orbits, boundary conditions on the lapse and shift are imposed such that the Arnowitt-Deser-Misner (ADM) and Komar mass (computed from the lapse) are equal, which is a necessary condition for the existence of a helical Killing vector. The expectation is that these conditions yield

$$\partial_t g_{ij} = \partial_t K = 0, \quad \partial_t \phi \approx \partial_t A_{ij} \approx 0. \tag{2}$$

It is not clear a priori how well $\partial_t \phi \approx 0$ and $\partial_t A_{ij} \approx 0$ are satisfied since only one necessary condition for the existence of the helical Killing vector has been enforced, namely the equality of the ADM and Komar mass. It would be interesting to check how much $\partial_t \phi$ and $\partial_t A_{ij}$ deviate from zero. Compared to Eq. (1), there are now additional errors in Eq. (2), which are related to the assumption of conformal flatness, and to the details of the construction. In particular the exact imposition of $\partial_t g_{ij} = 0$ and the method used for determining the orbital angular velocity of quasicircular orbits may introduce extra errors.

Another approach to construct binary BH initial data are puncture data [10], which are calculated using the conformal transverse traceless (CTT) decomposition [2,

11]. In this decomposition $\partial_t g_{ij} = 0$ cannot be achieved in general, while $\partial_t K = 0$ can always be imposed if a maximal slicing lapse is used. There still remains the gauge freedom to choose a shift that makes some of the time independence of a helical approximate Killing vector manifest. So far approximate helical Killing vectors have not explicitly been used in conjunction with puncture data. Instead, in order to obtain quasicircular orbits the effective potential method [12] was used in the past. In this method quasicircular orbits are identified with the extrema in the binding energy. For thin spherical shells of point particles it can be shown [13] that both the effective potential method as well as equality of Komar mass and ADM mass lead to the same identification of circular orbits. In general, however, it is not clear whether the effective potential method leads to an approximate Killing vector in some sense.

The angular velocity Ω at the innermost stable circular orbit (ISCO) computed from CTT puncture data with the effective potential method is almost twice as large as for Meudon data. Since the Ω found in the Meudon data is close to post-Newtonian predictions, the CTT method may be less reliable for ISCO data. It is important to note, however, that if quasicircular CTT data is computed for the separation predicted by the post-Newtonian and the Meudon CTS methods, then the discrepancy in Ω amounts to only a few percent [14]. This is an indication that it is not the CTT method by itself but rather the particular definition of the ISCO that is problematic. The remaining discrepancy may have to do with the different conformal decompositions used, but could also come from different boundary conditions, or the different ways in which circular orbits are found. The key difference between quasicircular data in the CTS and CTT methods is probably the construction of the extrinsic curvature. For CTS it is chosen such that $\partial_t g_{ij} = 0$, while for CTT the Bowen-York extrinsic curvature is used with the hope that the orbital parameters can be adjusted such that reasonable approximations to circular orbits are obtained. An analytical comparison of CTT data and CTS data can be found in [15].

In this paper we focus on CTT puncture data, for which we want to mention three reasons. First, the discrepancy between certain CTS and CTT approaches is not fully understood, but CTT appears to be more problematic. Second, in principle the puncture construction is significantly simpler than current implementations of CTS with excision. And third, to date all gravitational wave forms obtained numerically for binary BH inspirals are based on puncture initial data, see e.g. [16, 17, 18, 19, 20].

In the following, we investigate the quasicircularity of CTT puncture data numerically by asking whether such data possesses an approximate Killing vector. In our analysis we do not make changes to the standard CTT puncture data construction, but we try to find a lapse and shift such that Eq. (1) holds approximately. Concretely, we first compute a particular puncture data set for a quasicircular orbit as defined by the effective potential method. We then compute a maximal slicing lapse with novel boundary conditions that are derived from necessary conditions for the existence of a Killing vector, namely the equality of the Komar and ADM masses at infinity or the punctures. Given the puncture data and the lapse, we calculate a shift which minimizes $\partial_t g_{ij}$ in the sense that a certain divergence of the metric does not evolve in time, obtaining

$$\partial_t \partial_j g^{ij} = \partial_t K = 0, \quad \partial_t g_{ij} \approx \partial_t \phi \approx \partial_t A_{ij} \approx 0. \qquad (3)$$

In other words, we use the four degrees of freedom in lapse and shift to set the time derivatives of four metric and curvature quantities to zero. Compared to Eqs. (1) and (2), in addition to the assumptions about the Killing vector and conformal flatness there will be non-vanishing terms due to the choice of Bowen-York extrinsic curvature and the effective potential method. We therefore check numerically how small the time derivatives are that are supposed to vanish approximately in Eq. (3), in particular we use the Baumgarte-Shapiro-Shibata-Nakamura (BSSN) system [21, 22] of evolution equations to quantify the magnitude of the time derivatives.

The paper is organized as follows. In Sec. II we describe puncture data and briefly explain the methods we use to construct them numerically. Sec. III describes how the helical Killing vector assumption can be used to construct a lapse and shift for puncture data and presents numerical results. In Sec. IV we conclude with a discussion.

Notation. In this paper we use the standard $3 + 1$ decomposition of Einstein's equations, in which the 4-metric is written as

$$ds^2 = -\alpha^2 dt^2 + \bar{g}_{ij}(dx^i + \beta^i dt)(dx^j + \beta^j dt). \qquad (4)$$

Here $\bar{g}_{ij}$ is the intrinsic 3-metric on a $t = const$ hypersurface and α and β^i denote lapse and shift. Spatial components of tensors are denoted by Latin indices from the middle of the alphabet (e.g. i, j, ...). Latin letters from the beginning of alphabet are used for spacetime tensor indices. The extrinsic curvature is defined by

$$\bar{K}_{ab} = -\frac{1}{2}\pounds_n \bar{g}_{ab}, \qquad (5)$$

where n^a is the unit normal to the $t = const$ hypersurface. This implies that the time evolution vector is given by

$$\left(\frac{\partial}{\partial t}\right)^a = \alpha n^a + \beta^a. \qquad (6)$$

The 3-metric is decomposed into a conformal factor ϕ and a conformal 3-metric g_{ij}, such that

$$\bar{g}_{ij} = \phi^4 g_{ij}. \qquad (7)$$

The extrinsic curvature $\bar{K}_{ij}$ is split into its trace K and its tracefree part $\bar{A}^{ij}$ by writing it as

$$\bar{K}^{ij} = \bar{A}^{ij} + \frac{1}{3}\bar{g}^{ij}K. \tag{8}$$

As a rule, physical quantities have an overbar while conformal quantities do not, but lapse and shift are denoted by α and β^i and are not rescaled.

II. PUNCTURE DATA AND THE CTT DECOMPOSITION

Puncture data are computed using the conformal transverse traceless (CTT) decomposition. In the CTT decomposition $\bar{A}^{ij}$ is decomposed into

$$\bar{A}^{ij} = \phi^{-10}\left(A^{ij}_{TT} + LW^{ij}\right), \tag{9}$$

where A^{ij}_{TT} is an arbitrary transverse traceless piece (i.e. $\nabla_j A^{ij}_{TT} = 0$), and

$$LW^{ij} = \nabla^i W^j + \nabla^j W^i - \frac{2}{3}g^{ij}\nabla_k W^k \tag{10}$$

is the longitudinal piece. Then the Hamiltonian and momentum constraints become

$$\begin{aligned}\nabla^2\phi - \frac{1}{8}\phi R - \frac{1}{12}\phi^5 K^2 \\ +\frac{1}{8}\phi^{-7}(A^{ij}_{TT} + LW^{ij})(A^{kl}_{TT} + LW^{kl})g_{ik}g_{jl} &= 0\end{aligned} \tag{11}$$

and

$$\nabla_j LW^{ij} - \frac{2}{3}\phi^6\nabla^i K = 0, \tag{12}$$

which are elliptic equations for ϕ and W^i.

In the case of puncture data, the above CTS equations are further simplified by assuming that the 3-metric is conformally flat, i.e.

$$\bar{g}_{ij} = \phi^4\delta_{ij}. \tag{13}$$

In addition we set

$$K = 0 \tag{14}$$

so that the slice is maximal. We also assume that the transverse piece vanishes,

$$A^{ij}_{TT} = 0. \tag{15}$$

Analytic solutions to Eq. (12) are then given by

$$W^i = \sum_{A=1}^{2}\left[-\frac{1}{4r_A}\left(7P^i_A + s^i_A s_{Aj}P^j_A\right)\right] \tag{16}$$

and hence

$$\begin{aligned}\bar{K}^{ij} &= \bar{A}^{ij} = \phi^{-10}LW^{ij} \\ &= \phi^{-10}\sum_{A=1}^{2}\frac{3}{2r_A}\left(2P^{(i}_A s^{j)}_A - (\delta^{ij} - s^i_A s^j_A)s_{Ak}P^k_A\right)\end{aligned} \tag{17}$$

fulfills the momentum constraint. The notation here is as follows: The coordinate locations of the two BHs are denoted by (x_1, y_1, z_1) and (x_2, y_2, z_2) and we have introduced

$$r_A = \sqrt{(x-x_A)^2 + (y-y_A)^2 + (z-z_A)^2}. \tag{18}$$

and

$$s^i_A = (x-x_A, y-y_A, z-z_A)/r_A, \tag{19}$$

where the subscript A labels the BHs. The parameters P^i_A denote the momentum of each BH, and the ADM momentum at infinity is $P^i_1 + P^i_2$. On the other hand, the ADM momentum at the punctures, which represent the inner asymptotically flat ends of the hypersurface, vanishes by construction, i.e. the black holes 'do not move' when viewed from the inner ends which is a useful feature when looking for an approximate Killing vector. Choosing $P^i_1 + P^i_2 = 0$ we obtain data in coordinates where the net linear momentum vanishes at all three spatial infinities.

In order to find a conformal factor which fulfills the Hamiltonian constraint we make the ansatz

$$\phi = 1 + \frac{m_1}{2r_1} + \frac{m_2}{2r_2} + u, \tag{20}$$

which together with Eq. (11) leads to

$$\nabla^2 u + \frac{1}{8}\phi^{-7}LW^{ij}LW^{kl}g_{ik}g_{jl} = 0, \tag{21}$$

and we impose

$$\lim_{r\to\infty} u = 0 \tag{22}$$

as boundary condition on u. The equation for u has to be solved numerically. The solution u is finite and at least twice differentiable. It depends on the bare masses m_A, the momenta P_A and the separation $D = \sqrt{(x_1-x_2)^2 + (y_1-y_2)^2 + (z_1-z_2)^2}$.

In order to obtain quasicircular orbits, we use the parameters of Tab. I. The column denoted ISCO corresponds to the innermost stable circular orbit (ISCO) as determined by Baumgarte [23] with numerical values as in [24]. The Pre-ISCO column is a stable circular orbit found by Cook [12] transcribed into puncture data [14]. Note that for ease of comparison we use the same values for D, $|P_A|$, and m_A as in [14, 24], which were normalized such that the ADM mass at infinity should be unity. However, we find that M^{ADM}_∞ deviates from unity by roughly 1%. We thus estimate these parameters to be

TABLE I: Parameters used in order to obtain quasicircular orbits within the effective potential method, with Ω_{eff} denoting the inferred angular velocity. The column denoted ISCO corresponds to the innermost stable circular orbit (ISCO) as determined by Baumgarte, and the Pre-ISCO column corresponds to a stable circular orbit found by Cook. The $P_A = 0$ column is Brill-Lindquist data, i.e. two punctures with no momentum.

Parameter set	ISCO	Pre-ISCO	$P_A = 0$
D	2.303	3.698	3.698
$\|P_A\|$	0.3350	0.2148	0
m_A	0.4500	0.4775	0.5
M_∞^{ADM}	1.003	1.013	1
J_∞^{ADM}	0.7715	0.7944	0
$M_\infty^{ADM}\Omega_{eff}$	0.176	0.102	0

accurate to within about 1%, meaning that according to the effective potential method our orbits are not exactly circular. We were not able to obtain more accurate parameters from the literature.

Let us briefly discuss our numerical method. We solve the elliptic equations numerically using second order finite differencing and a multigrid elliptic solver. The code is a stand-alone version of BAM_Elliptic [25]. All grids have uniform resolution. Unless explicitly specified, all the results shown below are obtained with the outer boundary located at 12 and a finest resolution of $h = 0.0625$. As outer boundary conditions we use Robin conditions for all scalars, i.e. we assume that $u \propto v \propto 1/r$, where r is the distance to the center of mass. Here v determines the maximal slicing lapse (see Eq. (31) below). As boundary condition for the shift β_0^i (computed below) we use $\beta_0^i \propto 1/r^2$, which is a simplifying assumption that works reasonably well in practice. Since we are dealing with punctures, no inner boundaries are present. For the numerical work in this paper we consider non-spinning equal mass binaries with their center of mass at rest at the origin. The two BHs are positioned on the y-axis and their momenta point in the positive and negative x-directions, resulting in an angular momentum along the z-direction. After solving for u and v we observe second order convergence to zero in the Hamiltonian constraint and in $\partial_t K$, as expected. We also find second order convergence in the shift β^i after solving Eq. (55) below. The ADM and Komar integrals (defined in Sec. III below) at infinity are computed with volume integrals over u and v covering the numerical domain plus a correction for the missing volume such that the overall error is expected to fall off like one over the distance to the outer boundary squared. At the punctures, ADM masses and Komar integrals are obtained by fourth order interpolation of u and v onto the location of the punctures. From Fig. 1 we see that for $h = 0.0625$ the error in our masses at infinity is about 0.0005%, while the ADM and Komar integrals at the punctures have errors of 0.015% and 0.030% respectively.

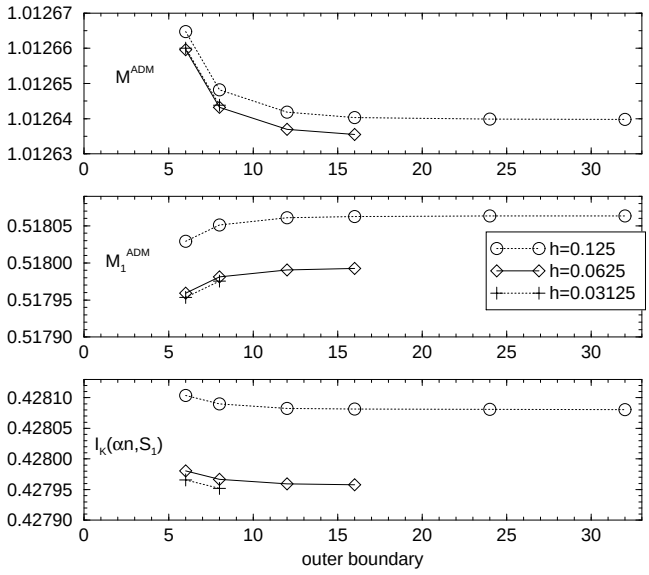

FIG. 1: Shown (from top to bottom) are the ADM mass at infinity, the ADM mass at one of the punctures and the Komar mass at one of the punctures, each at three resolutions h for different locations of the outer boundary, in the case of the Pre-ISCO parameter set. The error in the ADM mass at infinity at resolution $h = 0.0625$ is about 0.0005%, while the ADM and Komar masses at the punctures have errors of 0.015% and 0.030%,

III. HELICAL KILLING VECTORS

After solving for u, the puncture data are completely determined while lapse and shift are still arbitrary. We want to choose lapse and shift such that there is as little dynamical evolution as possible. This means we want a lapse and shift which satisfy

$$\partial_t g_{ij} = \partial_t \phi = \partial_t K = \partial_t \bar{A}_{ij} = 0 \tag{23}$$

as well as possible. If Eq. (23) really did hold, it would imply the existence of a Killing vector

$$\xi^a = \left(\frac{\partial}{\partial t}\right)^a = \alpha n^a + \beta^a, \tag{24}$$

which points along the time evolution vector. Since we are considering orbiting binaries this Killing vector would have to be a helical Killing vector, which means that at spatial infinity ($r \to \infty$)

$$n^a = T^a \quad \text{and} \quad \beta^a = \Omega \Phi^a \tag{25}$$

where T^a and Φ^a are the asymptotic time-translation and rotational Killing vectors at spatial infinity and Ω is the angular velocity with which the binary rotates.

A. Choice of lapse

In order to allow for the helical Killing vector (24) we now proceed by choosing a lapse such that

$$\partial_t K = 0 \tag{26}$$

which leads to the elliptic equation

$$\nabla^2(\alpha\phi) - \alpha\nabla^2\phi = \phi^5(\alpha\bar{K}_{ij}\bar{K}^{ij} + \beta^i\nabla_i K) \tag{27}$$

for the lapse. Note that this equation is valid for any g_{ij} and time independent K. We now use the specific form of puncture data and make the ansatz

$$\alpha\phi = 1 - \left(\frac{c_1 m_1}{2r_1} + \frac{c_2 m_2}{2r_2}\right) + v \tag{28}$$

for the lapse, where v is a finite correction. Together with Eqs. (27) and (11) this ansatz yields the elliptic equation

$$\nabla^2 v = \frac{7}{8}(\alpha\phi)\phi^{-8} L W_{ij} L W^{ij}, \tag{29}$$

which has to be solved numerically subject to the boundary condition

$$\lim_{r\to\infty} v = 0. \tag{30}$$

Combining Eqs. (20) and (28) yields

$$\alpha = \frac{1 - \left(\frac{c_1 m_1}{2r_1} + \frac{c_2 m_2}{2r_2}\right) + v}{1 + \frac{m_1}{2r_1} + \frac{m_2}{2r_2} + u}. \tag{31}$$

Hence we obtain

$$\lim_{r\to\infty} \alpha = 1 \tag{32}$$

as boundary condition at spatial infinity, which is what one wants in asymptotically Minkowskian coordinates. The value at each puncture is

$$\lim_{r_A\to 0} \alpha = -c_A, \tag{33}$$

that is, our ansatz for the lapse (28) introduces the freedom to pick the value of the lapse at the inner asymptotically flat ends.

This freedom turns out to be essential when trying to satisfy the mass condition for a helical Killing vector field. But let us first discuss the situation for a single puncture without momentum, i.e. the case of $P_1^i = P_2^i = m_2 = K_{ij} = u = 0$, which corresponds to a Schwarzschild BH in isotropic coordinates. Of course, the Schwarzschild spacetime is static and thus has a Killing vector ξ^a so that we can ask for which c_1 Eqs. (23) and (24) do indeed hold. It is easy to see that

$$\alpha = 1 \quad \text{everywhere}, \tag{34}$$

which corresponds to $v = 0$ and $c_1 = -1$, fulfills Eq. (29) so that $\partial_t K = 0$ holds. If in addition we choose $\beta^i = 0$, we also get $\partial_t g_{ij} = \partial_t \phi = 0$. However $\partial_t \bar{A}_{ij} \neq 0$, and hence $c_1 = -1$ is not a good choice since it leads to an evolving $\bar{A}_{ij}$ even in the case of the static Schwarzschild spacetime.

Another possibility obtained from $c_1 = 1$ and $v = 0$ is

$$\alpha = \frac{1 - \frac{m_1}{2r_1}}{1 + \frac{m_1}{2r_1}}, \tag{35}$$

which also yields $\partial_t K = 0$. This is the standard lapse of isotropic coordinates. If we again choose $\beta^i = 0$ we find that Eqs. (23) and (24) are now satisfied. Therefore $c_1 = 1$ is a good choice for a single BH. It turns out that for $c_1 = 1$ the Komar mass $I_K(\alpha n, S_\infty)$ (see Eq. (36) below) computed from α equals the ADM mass of the BH. This is not true for $c_1 = -1$ for which $I_K(\alpha n, S_\infty) = 0$.

Let us return to the general case of binary BH data and discuss what it means to impose equality of the Komar and ADM masses. The binary puncture data that we are considering may not possess a helical Killing vector ξ^a, but if they did then the Komar integral [26, 27, 28]

$$I_K(\xi, S) = -\frac{1}{8\pi}\int_S \bar{\epsilon}_{abcd}\bar{\nabla}^c\xi^d \tag{36}$$

integrated over any closed 3-surface S containing the punctures would yield the same answer. Furthermore if we choose S to be a sphere at $r \to \infty$ and if ξ^a is normalized such that

$$\lim_{r\to\infty} \xi^a n_a = -1, \tag{37}$$

then

$$I_K(\xi, S) = M_\infty^{ADM} - 2\Omega J_\infty^{ADM} \tag{38}$$

is expected to hold as an immediate generalization of [27]. Here M_∞^{ADM} and J_∞^{ADM} are the ADM mass and angular momentum at spatial infinity ($r \to \infty$) given by

$$M_\infty^{ADM} = P_{\mu\ \infty}^{ADM} P_{\nu\ \infty}^{ADM} \eta^{\mu\nu}, \tag{39}$$

$$P_{0\ \infty}^{ADM} = \frac{1}{16\pi}\int_{S_\infty} (\bar{g}_{ij,i} - \bar{g}_{ii,j}) d\bar{S}^j, \tag{40}$$

$$P_{i\ \infty}^{ADM} = \frac{1}{8\pi}\int_{S_\infty} (\bar{K}_{ij} - K\eta_{ij}) d\bar{S}^j, \tag{41}$$

and

$$J_\infty^{ADM} = \frac{1}{8\pi}\int_{S_\infty} (\bar{K}_{ij}\Phi^j - K\Phi_i) d\bar{S}^i. \tag{42}$$

Note that the normalization condition (37) requires that $\alpha \to 1$ for $r \to \infty$.

If we insert ξ^a as given in Eq. (24) into Eq. (36) we obtain

$$\begin{aligned} I_K(\xi, S) &= I_K(\alpha n, S) + I_K(\beta, S) \\ &= \frac{1}{4\pi}\int_S \bar{\nabla}_i \alpha d\bar{S}^i - \frac{1}{4\pi}\int_S \bar{K}_{ij}\beta^i d\bar{S}^j. \end{aligned} \tag{43}$$

Using Eq. (25) we find that the second term integrated at $r \to \infty$ is

$$I_K(\beta, S_\infty) = -2\Omega \frac{1}{8\pi} \int_{S_\infty} \bar{K}_{ij} \Phi^j d\bar{S}^i = -2\Omega J_\infty^{ADM}. \tag{44}$$

Therefore combining Eqs. (38), (43) and (44) the condition

$$I_K(\alpha n, S_\infty) = M_\infty^{ADM} \tag{45}$$

must hold if the helical Killing vector of Eq. (24) exists.

We can now address the question what the values $-c_A$ of the lapse at the punctures should be. Since we are interested in the case where a helical Killing vector exists (at least approximately), we should pick c_A such that Eq. (45) is fulfilled, otherwise ξ^a cannot be a Killing vector. Since Eq. (45) is just one condition on in principle two unknowns, we also set $c_1 = c_2$ so that the lapse has the same value at each puncture. This is justified by the fact that in our numerical computations we only study equal mass binaries with $m_1 = m_2$. Of course Eq. (45) is only a necessary condition for a Killing vector. To test whether a Killing vector really exists, we have to check how well Eq. (23) is fulfilled.

We summarize our numerical results in Tab. II. Given the ISCO and Pre-ISCO parameters described in Tab. I, we iterate c_A until $I_K(\alpha n, S_\infty) = M_\infty^{ADM}$. Tab. II gives the values for c_A for which this can indeed be achieved. Since the lapse has now been fixed, we proceed to check two other relations, namely the mass equality at the punctures (as opposed to infinity) and the angular velocity Ω predicted by the Komar integral.

Note that Eq. (38) can be used to compute the angular velocity Ω if the Komar integral $I_K(\xi, S)$ is evaluated on a surface $S \neq S_\infty$. Let us use Eq. (43) to calculate $I_K(\xi, S_p)$ for $S_p = S_1 \cup S_2$, where S_1 and S_2 are infinitesimally small spheres around each puncture. If we set β^i to zero at the punctures (an assumption which will be justified below in Sec. III B), the shift term in Eq. (43) does not contribute and we find

$$\begin{aligned} I_K(\xi, S_p) &= I_K(\alpha n, S_1) + I_K(\alpha n, S_2) \\ &= m_1 \left[\frac{1+c_1}{2} + \frac{v_1 + c_1 u_1}{2} + \frac{(c_1 - c_2) m_2}{4D} \right] \\ &\quad + m_2 \left[\frac{1+c_2}{2} + \frac{v_2 + c_2 u_2}{2} + \frac{(c_2 - c_1) m_1}{4D} \right], \end{aligned} \tag{46}$$

where u_A and v_A are the values of u and v at puncture A. Note that $c_1 = c_2$ implies that there is no explicit dependence on D, but u_A and v_A depend on D. If ξ^a is a Killing vector, $I_K(\xi, S_p)$ should have the same value as in Eq. (38), which in turn implies

$$\Omega = \frac{M_\infty^{ADM} - I_K(\xi, S_p)}{2 J_\infty^{ADM}}. \tag{47}$$

Comparing Tabs. I and II we see that the angular velocity (47) of the binary is very close to what is found with the effective potential method.

TABLE II: The value of the lapse at the puncture for the three parameter sets of table I is chosen such that Eq. (45) holds. We find that then Eq. (48) also approximately holds. In addition the Ω of Eq. (47) is close to what the effective potential method predicts, and up to numerical accuracy $\Omega = \Omega_\beta$ for Ω_β introduced in Sec. III B.

Parameter set	ISCO	Pre-ISCO	$P_A = 0$
c_A	0.726	0.829	1.000
M_∞^{ADM}	1.003	1.013	1.000
$I_K(\alpha n, S_\infty)$	1.003	1.013	1.000
M_A^{ADM}	0.514	0.518	0.534
$I_K(\alpha n, S_A)$	0.372	0.428	0.500
$c_A M_A^{ADM}$	0.373	0.430	0.534
$\frac{c_A M_A^{ADM} - I_K(\alpha n, S_A)}{c_A M_A^{ADM}}$	0.0027	0.0047	0.0637
$M_\infty^{ADM} \Omega$	0.168	0.100	0.000
$M_\infty^{ADM} \Omega_\beta$	0.168	0.100	0.000

A further check is provided by the analogue

$$I_K(\alpha n, S_A) = c_A M_A^{ADM} \tag{48}$$

to Eq. (45). Here the ADM mass of each puncture is given by

$$M_A^{ADM} = m_A(1 + u_A) + \frac{m_1 m_2}{2D}, \tag{49}$$

and the factor c_A comes from the fact that at the puncture ξ^a is normalized such that $\xi^a n_a = c_A$, which differs from the standard normalization in Eq. (37). As one can see in Tab. II our numerical results for M_A^{ADM} and $I_K(\alpha n, S_A)$ approximately satisfy Eq. (48) in the case of quasicircular orbits, while for the $P_A = 0$ data Eq. (48) is violated. Yet even for quasicircular orbits the deviation from Eq. (48) is larger than our numerical errors, but the parameters of Tab. I used to put the punctures into quasicircular orbits (according to the effective potential method) are not very accurate. We believe that these parameters are accurate up to 1% error, hence some deviations from Eq. (48) are expected. In future work we plan to construct quasicircular orbits within our numerical method, which involves varying P_A^i, and it should be possible to define P_A^i for quasicircular orbits by imposing Eq. (48). For the parameters used in the present work, we conclude that the one parameter freedom of the lapse at the puncture allows us to find a lapse that is approximately compatible with the two necessary conditions (45) and (48) for a helical Killing vector.

A plot of the lapse is shown in Fig. 2 for two punctures located on the y-axis for the case of the Pre-ISCO parameter set of Tab. I.

B. Choice of shift

In Sec. III A we have chosen the lapse such that $\partial_t K = 0$. Similarly we would like to choose a shift which results

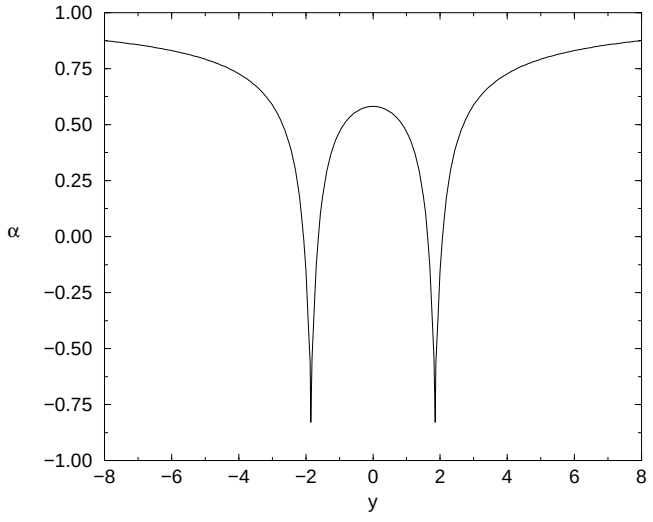

FIG. 2: The lapse α along the y-axis for the Pre-ISCO data set. The punctures are on the y-axis at $y = \pm 1.849$.

in $\partial_t g_{ij} = 0$. In general (if the conformal factor is chosen such that $\partial_t \det g_{ij} = 0$), we have

$$\partial_t g_{ij} = -2\alpha\phi^{-4}\bar{A}_{ij} + L\beta_{ij}. \tag{50}$$

Note however that $L\beta_{ij}$ is by definition purely longitudinal, so that the left hand side can only be zero if $2\alpha\phi^{-4}\bar{A}_{ij}$ is purely longitudinal as well. The CTS construction enforces this feature by exchanging the role of $\bar{A}_{ij}$ and $\partial_t g_{ij}$, i.e. the time derivative of the metric is treated as free data that defines the extrinsic curvature through

$$\bar{A}_{ij} = \frac{1}{2\alpha\phi^{-4}}\left(L\beta_{ij} - \partial_t g_{ij}\right). \tag{51}$$

For maximal slicing and vanishing time derivative of the metric one obtains an elliptic equation for the shift by taking a divergence of (51) and using the momentum constraint which leads to

$$\nabla_j L\beta^{ij} = L\beta^{ij}\nabla_j \log\left(\alpha\phi^{-6}\right). \tag{52}$$

In the CTS construction these are three of five coupled equations for ϕ, α, and β^i.

However, for puncture data with maximal slicing, ϕ, α, and $\bar{A}_{ij}$ are determined independently of the shift, and in particular $2\alpha\phi^{-4}\bar{A}_{ij}$ will not be purely longitudinal in general. In fact, for the puncture data we are considering here,

$$2\alpha\phi^{-4}\bar{A}_{ij} = 2\alpha\phi^{-6}LW_{ij}, \tag{53}$$

so that $2\alpha\phi^{-4}\bar{A}_{ij}$ is the product of a longitudinal piece and a scalar function.

But we can still determine a shift that completely removes the longitudinal piece from the time derivative of the metric. Concretely, in order to find the longitudinal piece $L\beta^{ij}$ of Eq. (53) for puncture data, let us make the ansatz

$$2\alpha\phi^{-6}LW^{ij} = L\beta^{ij} + v^{ij}_{TT}, \tag{54}$$

where v^{ij}_{TT} is a possible transverse traceless piece with $\nabla_j v^{ij}_{TT} = 0$. By taking the divergence of Eq. (54) we find the elliptic equation

$$\nabla_j L\beta^{ij} = \nabla_j\left(2\alpha\phi^{-6}LW^{ij}\right), \tag{55}$$

which has a unique solution for β^i for given boundary conditions (compare with Eq. (52) for CTS). Once we have found β^i, we can then determine v^{ij}_{TT} from Eq. (54). Since we are interested in a binary configuration in corotating coordinates we should adopt

$$\lim_{r\to\infty}\beta^i = \Omega_\beta \Phi^i \tag{56}$$

as boundary conditions for β^i at spatial infinity. Here Φ^i is the asymptotic rotational Killing vector pointing along the direction of rotation and Ω_β is the angular velocity of the binary. Let us split the shift into the two pieces

$$\beta^i = \beta^i_0 + \beta^i_{rot}, \tag{57}$$

where we have introduced the rotational piece

$$\beta^i_{rot} = \epsilon^i_{jk} x^j \Omega^k_\beta \tag{58}$$

and a piece with

$$\lim_{r\to\infty}\beta^i_0 = 0. \tag{59}$$

The benefit of this split is that $L\beta^{ij}_{rot} = 0$, so that if β^i_0 fulfills Eq. (55) with boundary condition (59), β^i of Eq. (57) immediately fulfills Eq. (55) with boundary condition (56). We have numerically solved for β^i_0 and then added a rotational piece of the form (58) such that $\beta^i = 0$ at each puncture. This is a very desirable property since punctures have no linear momentum when viewed from the asymptotically flat region at the puncture, so that the natural choice for the shift is indeed zero. The shift for the Pre-ISCO parameter set of Tab. I is shown in Fig. 3. Notice that β^i is linear for large r in agreement with boundary condition (56). It turns out that up to the accuracy of our numerical computation, the Ω_β required to achieve $\beta^i = 0$ at each puncture is equal to the Ω computed from Eq. (47). We want to stress here that $\Omega_\beta = \Omega$ is another necessary condition for a Killing vector (see appendix A) and not expected to hold a priori for puncture data.

In Fig. 4 we show plots of the three terms in Eq. (54). We find that v^{ij}_{TT} in Eq. (54) is indeed non-zero. Hence Eq. (50) becomes

$$\partial_t g_{ij} = -2\alpha\phi^{-6}LW_{ij} + L\beta_{ij} = -v^{TT}_{ij}, \tag{60}$$

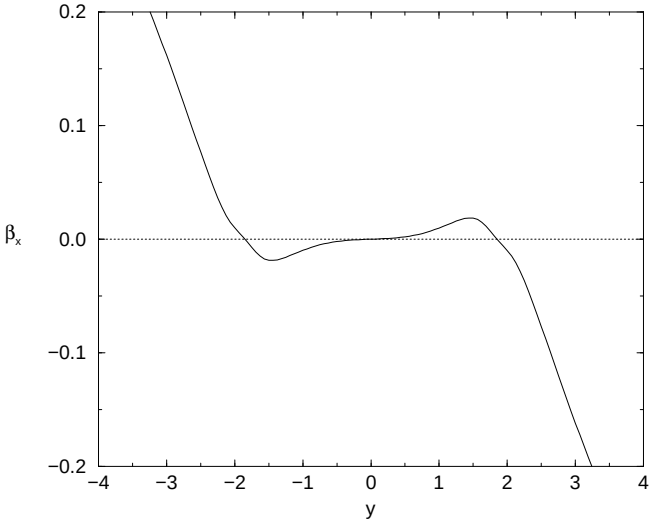

FIG. 3: The shift β^x for Pre-ISCO data along the y-axis, which connects the two punctures. At each puncture β^x vanishes.

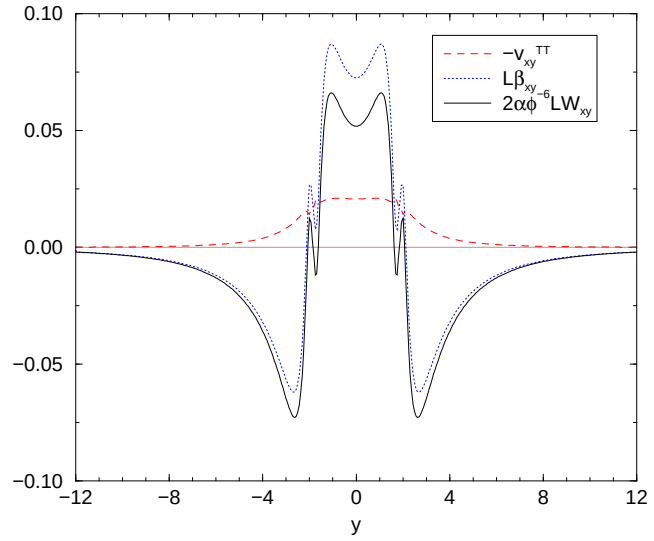

FIG. 4: The three terms in Eq. (54) for Pre-ISCO data.

and $\partial_t g_{ij} = 0$ cannot be achieved for puncture data. Note however that v^{ij}_{TT} is smaller than $L\beta^{ij}$, and that $2\alpha\phi^{-6}LW^{ij}$ is purely longitudinal for large r. Thus $\partial_t g_{ij}$ is at least reduced by the above choice of β^i. The maximum value is

$$\max \partial_t g_{ij} = 2 \times 10^{-2}/M^{ADM}. \tag{61}$$

Hence the smallest timescale on which g_{ij} evolves is $T_{g_{ij}} = 2\pi(1/\max \partial_t g_{ij}) \sim 300M^{ADM}$ which is longer than the dynamical timescale given by $T_{dyn} = 2\pi/\Omega \sim 60M^{ADM}$. This means that g_{ij} is approximately constant up to an error of at most $T_{dyn}/T_{g_{ij}} \sim 20\%$ in the center and much less away from the punctures.

So far we have only addressed the time derivatives of K and g_{ij}. We will now use the BSSN evolution equations to investigate the remaining time derivatives. Recall that BSSN introduce the additional variables

$$\tilde{\Gamma}^i = -\partial_j \tilde{\gamma}^{ij}, \tag{62}$$

where the BSSN metric $\tilde{\gamma}_{ij} = g_{ij} = \delta_{ij}$ on the initial slice for the case of conformally flat puncture data. Using Eqs. (50) and (53) we obtain

$$\partial_t \tilde{\Gamma}^i = -\nabla_j \partial_t g^{ij} = \nabla_j L\beta^{ij} - \nabla_j \left(2\alpha\phi^{-6}LW^{ij}\right). \tag{63}$$

Thus, when Eq. (55) is fulfilled we have

$$\partial_t \tilde{\Gamma}^i = 0, \tag{64}$$

so that $\tilde{\Gamma}^i$ does not evolve with our choice of shift. Put differently, we have three free functions available in terms of the shift vector. This does not suffice to set $\partial_t g_{ij} = 0$ for puncture data, but we can impose the so-called Gamma-freezing condition (64) [17, 29], which we have obtained here by constructing a shift for CTT data motivated by CTS data.

The time derivatives of the remaining variables have to be studied numerically. We will do this next for the Pre-ISCO parameter set of Tab. I. First we look at the variable

$$\varphi = \log \phi, \tag{65}$$

which BSSN introduce by decomposing the physical metric as $\bar{g}_{ij} = e^{4\varphi}\tilde{\gamma}_{ij}$. Numerically we find that $\partial_t \varphi$ is very close to zero. The maximum value is

$$\max \partial_t \varphi = \max \frac{\partial_t \phi}{\phi} = 5 \times 10^{-3}. \tag{66}$$

This means that ϕ evolves on a timescale $T_{phi} = 2\pi(\phi/\partial_t\phi) > 1200M^{ADM}$, which is much longer than the dynamical timescale given by $T_{dyn} \sim 60M^{ADM}$.

Finally, Fig. 5 shows the BSSN variable $\tilde{A}_{ij} = e^{-4\varphi}\bar{A}_{ij} = \phi^{-4}\bar{A}_{ij}$, and its time derivative. We see that $\partial_t \tilde{A}_{ij}$ does not vanish. In fact for some components such as $\tilde{A}_{yy}$, $\partial_t \tilde{A}_{ij}$ is not much smaller then $\tilde{A}_{ij}$ itself, while the time derivative of the dominant component $\tilde{A}_{xy}$ is small. This implies that puncture data cannot have a helical Killing vector. However as we can see in Fig. 6, $\partial_t \tilde{A}_{ij}$ is reduced by our choice of lapse and shift when compared to the case of $\alpha = 1$ and $\beta^i = 0$, which is often used as initial data for lapse and shift when evolving with dynamical gauge conditions. Hence our choice of lapse and shift at least brings us closer to the situation of minimal evolution.

IV. DISCUSSION

We have shown that puncture data for quasicircular binary BHs obtained in the CTT framework with the

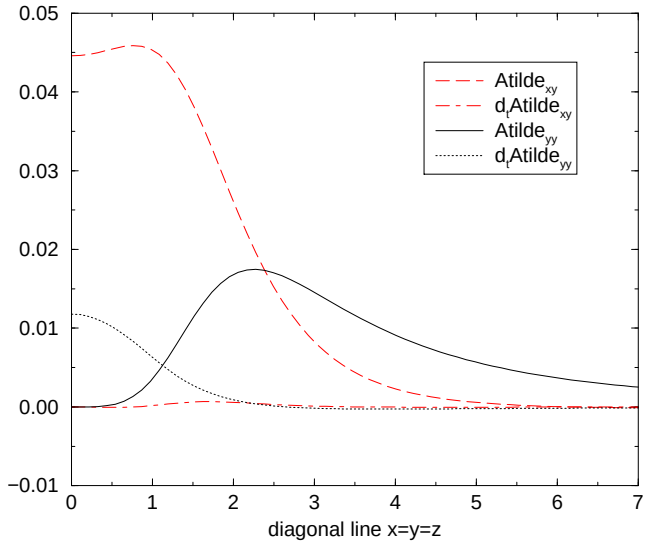

FIG. 5: Selected components of $\tilde{A}_{ij}$ and their time derivatives along the diagonal $x = y = z$ for Pre-ISCO data.

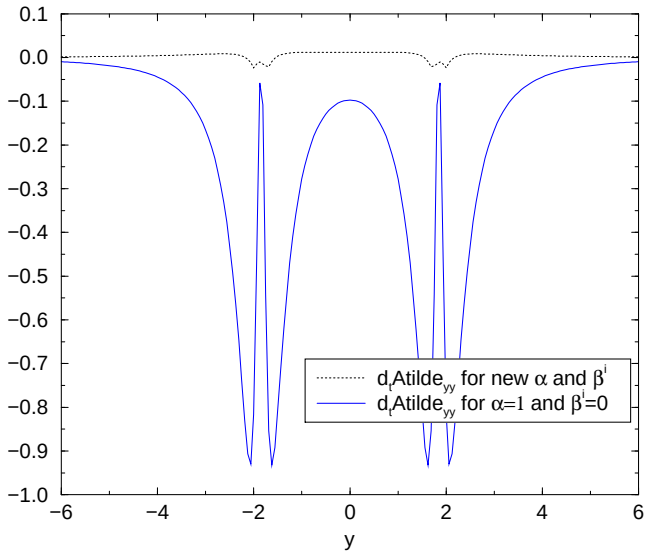

FIG. 6: The time derivative of $\tilde{A}_{yy}$ for α and β^i computed from Eqs. (27) and (55) is much smaller than for $\alpha = 1$ and $\beta^i = 0$ for Pre-ISCO data.

effective potential method allows a special gauge choice that realizes some of the necessary conditions for the existence of an approximate helical Killing vector field. Introducing a free parameter for the lapse at the punctures we can satisfy the condition that the Komar and ADM mass agree at spatial infinity. Since there are no further free parameters in our gauge choice, it becomes a non-trivial fact that the Komar and ADM mass also approximately agree at the punctures, and that the angular velocity given by three different methods agree within a certain accuracy. The angular velocity Ω_β determined by the shift that vanishes at the punctures is equal to the angular velocity Ω inferred by assuming that the Komar integral can be evaluated on any surface containing the punctures, and both Ω_β and Ω agree approximately with the angular velocity prescribed by the effective potential method.

Our gauge choice controls some of the time derivatives of the metric variables, $\partial_t K = 0$ and $\partial_t \partial_j g^{ij} = 0$. Furthermore, we find that ϕ varies on a timescale much larger than the orbital timescale and that g_{ij} varies on a timescale which is at least five times the orbital timescale. The magnitude of $\partial_t \bar{A}_{ij}$ is reduced when we compare to the case of lapse $\alpha = 1$ and zero shift, but it still varies on the orbital timescale.

One conclusion to draw from our results is that quasicircular puncture data is not as far from possessing a helical Killing vector as one might have expected. This is an important observation since to date all gravitational wave forms obtained for binary BH mergers are based on such initial data.

Note that in the present work we have used parameters for quasicircular puncture data found in the literature. It should now be possible to construct sequences of quasicircular orbits based on the Komar and ADM mass equalities and compare with the effective potential method. At a given separation D, one has to vary the linear momenta P^i_A and the constants c_A for the lapse at the punctures until both Eqs. (45) and (48) are satisfied. The variation to find quasicircular orbits has to keep, for example, the ADM masses at the punctures constant (cmp. [30]), which would be particularly natural in our approach.

Another direction for future work is to perform evolutions of puncture data with the initial gauge derived here. Note that this is not entirely straight-forward because the lapse crosses from positive to negative values near the apparent horizon, which is also true for the Meudon data sets construct in the CTS framework, but in that case an isometry condition is imposed. It is not clear whether there are numerical problems related to a negative lapse, even if one applies BH excision techniques, but this is certainly worth exploring.

Finally, an immediate question is whether one can perhaps modify the extrinsic curvature of the puncture data to better control $\partial_t \bar{A}_{ij}$. Puncture data provides a genuine technical simplification over methods with excision, but so far it has not been possible to construct thin sandwich puncture data in order to improve the extrinsic curvature. One aspect of the problem becomes already apparent when considering maximal slicing of Schwarzschild, which is known analytically [31]. It is not hard to see that demanding $\partial_t \bar{g}_{ij} = 0$ for all t immediately leads to the standard isotropic coordinates with negative lapse at the puncture and vanishing shift [32]. The conclusion is that there is no maximal slicing of Schwarzschild with static metric components and positive lapse. On the other hand, in [17] evolutions of Schwarzschild with

positive lapse have been performed that display an approximate Killing vector, therefore the existence of thin sandwich puncture data has not been ruled out.

Acknowledgments

It is a pleasure to thank Abhay Ashtekar and Greg Cook for discussions. We acknowledge the support of the Center for Gravitational Wave Physics funded by the National Science Foundation under Cooperative Agreement PHY-01-14375. This work was also supported by NSF grants PHY-02-18750 and PHY-98-00973.

APPENDIX A: INTEGRAL I_K DEFINED WITHOUT A KILLING VECTOR

If the conformal factor is chosen such that $\partial_t \det g_{ij} = 0$, the evolution equations for ϕ, g_{ij} and K are

$$
\begin{aligned}
6\partial_t \log\phi &= -\alpha K + \bar\nabla_i \beta^i, && \text{(A1)}\\
\partial_t g_{ij} &= \phi^{-4}(\bar L\beta_{ij} - 2\alpha \bar A_{ij}) && \text{(A2)}\\
\partial_t K &= \bar\nabla^2\alpha + \alpha \bar A_{ij}\bar A^{ij} + \alpha K^2 + \beta^i\partial_i K. && \text{(A3)}
\end{aligned}
$$

If we solve Eqs. (A1) and (A2) for αK and $\bar A_{ij}$ respectively and insert the results into Eq. (A3) we obtain

$$
\begin{aligned}
\bar\nabla^i\left(\bar\nabla_i\alpha - \bar K_{ij}\beta^j\right) &= -\bar A^{ij}\phi^4\partial_t g_{ij} - \partial_t K\\
&\quad - \left(6\partial_t\log\phi - \frac{2}{3}\bar\nabla_i\beta^i\right)K, && \text{(A4)}
\end{aligned}
$$

where we have made use of the momentum constraint. Now note that the term in parentheses on the left hand side is the same as in Eq. (43). This suggests to define the volume integral

$$
\begin{aligned}
I_V &= \frac{1}{4\pi}\int_V \bar\nabla^i\left(\bar\nabla_i\alpha - \bar K_{ij}\beta^j\right)\\
&= \frac{1}{4\pi}\int_V\Bigg[-\bar A^{ij}\phi^4\partial_t g_{ij} - \partial_t K\\
&\quad - \left(6\partial_t\log\phi - \frac{2}{3}\bar\nabla_i\beta^i\right)K\Bigg]. && \text{(A5)}
\end{aligned}
$$

Next, let us define $I_K(\alpha n+\beta, S)$ by the right hand side of Eq. (43) even if no Killing vector ξ exists. Now, if the volume V in Eq. (A5) is bounded by the surfaces S_∞ and S_p we find that

$$
I_K(\alpha n+\beta, S_\infty) - I_K(\alpha n+\beta, S_p) = I_V, \qquad \text{(A6)}
$$

i.e. the value of $I_K(\alpha n+\beta, S)$ in general does depend on the surface S on which it is evaluated. If, however, $\alpha n^a+\beta^a$ is a Killing vector, I_V vanishes and $I_K(\alpha n+\beta, S)$ does not depend on S.

We now adjust the shift such that $\beta^i = 0$ on S_p and $\beta^i = \Omega_\beta \Phi^i$ on S_∞, then Eq. (A6) becomes

$$
I_K(\alpha n, S_\infty) - 2\Omega_\beta J^{ADM}_\infty - I_K(\alpha n, S_p) = I_V. \qquad \text{(A7)}
$$

Choosing the lapse such that Eq. (45) is satisfied, yields

$$
\Omega_\beta = \frac{M^{ADM}_\infty - I_K(\xi, S_p) - I_V}{2J^{ADM}_\infty}. \qquad \text{(A8)}
$$

Hence Ω_β and Ω of Eq. (47) differ by the term I_V, which vanishes if $\alpha n^a + \beta^a$ is a Killing vector. Another necessary condition for the existence of a Killing vector is thus $\Omega_\beta = \Omega$. For punctures with our choice of lapse we have $K = \partial_t K = 0$, so that all terms involving K in I_V of Eq. (A5) vanish, the term with $\partial_t g_{ij}$ in I_V however may not integrate to zero, so that $\Omega_\beta = \Omega$ is non-trivial for puncture data.

[1] B. Schutz, Class. Quantum Grav. **16**, A131 (1999).
[2] G. B. Cook, Living Reviews in Relativity **2000**, 5 (2000).
[3] W. Tichy, B. Brügmann, M. Campanelli, and P. Diener, Phys. Rev. D **67**, 064008 (2003), gr-qc/0207011.
[4] J. R. Wilson and G. J. Mathews, Phys. Rev. Lett. **75**, 4161 (1995).
[5] J. W. York, Phys. Rev. Lett. **82**, 1350 (1999).
[6] E. Gourgoulhon, P. Grandclement, and S. Bonazzola, Phys. Rev. D **65**, 044020 (2001), gr-qc/0106015.
[7] P. Grandclement, E. Gourgoulhon, and S. Bonazzola, Phys. Rev. D **65**, 044021 (2001), gr-qc/0106016.
[8] H. P. Pfeiffer, G. B. Cook, and S. A. Teukolsky, Phys. Rev. **D66**, 024047 (2002), gr-qc/0203085.
[9] G. B. Cook, Phys. Rev. **D65**, 084003 (2002), gr-qc/0108076.
[10] S. Brandt and B. Brügmann, Phys. Rev. Lett. **78**, 3606 (1997).
[11] J. W. York, J. Math. Phys. **14**, 456 (1973).
[12] G. B. Cook, Phys. Rev. D **50**, 5025 (1994).
[13] M. Skoge and T. Baumgarte, Phys. Rev. D **66**, 107501 (2002).
[14] J. Baker, M. Campanelli, C. O. Lousto, and R. Takahashi, Phys. Rev. **D65**, 124012 (2002), astro-ph/0202469.
[15] P. Laguna (2003), in preparation.
[16] M. Alcubierre, W. Benger, B. Brügmann, G. Lanfermann, L. Nerger, E. Seidel, and R. Takahashi, Phys. Rev. Lett. **87**, 271103 (2001), gr-qc/0012079.
[17] M. Alcubierre, B. Brügmann, P. Diener, M. Koppitz, D. Pollney, E. Seidel, and R. Takahashi, Phys. Rev. D **67**, 084023 (2003), gr-qc/0206072.
[18] J. Baker, M. Campanelli, and C. O. Lousto, Phys. Rev. **D65**, 044001 (2002), gr-qc/0104063.
[19] J. Baker, B. Brügmann, M. Campanelli, C. O. Lousto,

and R. Takahashi, Phys. Rev. Lett. **87**, 121103 (2001), gr-qc/0102037.
[20] J. Baker, M. Campanelli, C. O. Lousto, and R. Takahashi (2003), astro-ph/0305287.
[21] M. Shibata and T. Nakamura, Phys. Rev. D **52**, 5428 (1995).
[22] T. W. Baumgarte and S. L. Shapiro, Physical Review D **59**, 024007 (1999), gr-qc/9810065.
[23] T. W. Baumgarte, Phys. Rev. D **62**, 024018 (2000), gr-qc/0004050.
[24] J. Baker, B. Brügmann, M. Campanelli, and C. O. Lousto, Class. Quantum Grav. **17**, L149 (2000).
[25] B. Brügmann, Ann. Phys. (Leipzig) **9**, 227 (2000), gr-qc/9912009.
[26] A. Komar, Phys. Rev. **113**, 934 (1959).
[27] A. Ashtekar and A. Magnon-Ashtekar, J. Math. Phys. **20**, 793 (1979).
[28] R. M. Wald, *General Relativity* (The University of Chicago Press, Chicago, 1984).
[29] M. Alcubierre and B. Brügmann, Phys. Rev. D **63**, 104006 (2001), gr-qc/0008067.
[30] B. D. Baker (2002), gr-qc/0205082.
[31] F. Estabrook, H. Wahlquist, S. Christensen, B. DeWitt, L. Smarr, and E. Tsiang, Phys. Rev. D **7**, 2814 (1973).
[32] B. Reimann, Master's thesis, Universität Potsdam (2003).